Photodecomposition of Nitrite and Undissociated Nitrous Acid in Aqueous Solution

Michael Fischer and Peter Warneck*

Max-Planck-Institut für Chemie, 55020 Mainz, Germany

Received: June 6, 1996; In Final Form: September 3, 1996[⊗]

Quantum yields of phenol and nitrate, produced by photodecomposition in aqueous solutions of NO_2^- and HNO_2 in the presence of benzene as scavenger for OH radicals, have been determined as a function of wavelength between 280 and 390 nm. The production of phenol was used to calculate primary OH quantum yields. For NO_2^- photolysis at pH 6 Φ_1(OH) was found to decrease with increasing wavelength from 0.069 ± 0.008 at 280 nm to 0.022 ± 0.004 at 390 nm, in agreement with previous data. The OH quantum yield Φ_2(OH) for the photolysis of HNO_2 at pH 2 was essentially constant over the entire wavelength range with $\Phi_2 = 0.35 \pm 0.02$ (2σ). Quantum yields for NO_3^- are comparable in magnitude to those of phenol, indicating that NO as primary product is largely oxidized to nitrate. The most likely conversion processes are reactions of NO with O_2^- (pH 6), the latter resulting from the oxidation of benzene, to form peroxynitrous acid, which undergoes thermal decomposition, and of NO_2 with HO_2 (pH 2) to form peroxynitric acid, which reacts further with HNO_2. The rate of NO_3^- production decreases with time in the photolysis of NO_2^-, whereas it increases in the photolysis of HNO_2, and these features remain unexplained.

Introduction

The nitrite anion (NO_2^-) and undissociated nitrous acid (HNO_2) in aqueous solution undergo photodecomposition following the absorption of light in the 300−400 nm wavelength region, where both species feature moderately intense absorption bands. Photodecomposition products and quantum yields are of interest to environmental chemistry, because the wavelength range of absorption overlaps that of the solar spectrum and nitrite is present in atmospheric water drops[1,2] as well as in surface waters.[3] Earlier experimental studies by Treinin and Hayon[4] and Strehlow and Wagner[5] have established that the photolysis of nitrite produces mainly NO and the O^- radical, which at pH ≤ 11.9 (the pK_a value for OH/O^-) is rapidly protonated and converted to the OH radical. The possibility that NO_2 and a hydrated electron are formed in a parallel process has not been fully discounted, but these are minor products. The photolysis of HNO_2 (p$K \approx 3.2$) also has been demonstrated to generate OH radicals.[6,7] The absorption spectrum of HNO_2 in aqueous solution is similar to that of HNO_2 in the gas phase. In this case NO and OH are the only photodissociation products.[8,9] Accordingly, we may write

$$NO_2^- + h\nu\ (+H^+) \rightarrow NO + OH \qquad \text{(R1)}$$

$$NO_2^- + h\nu \rightarrow NO_2 + e_{aq}^- \qquad \text{(R1a)}$$

$$HNO_2 + h\nu \rightarrow NO + OH \qquad \text{(R2)}$$

In the absence of other solutes, OH undergoes a rapid secondary reaction with nitrite or nitrous acid to form NO_2, which largely combines with NO to form N_2O_3.[4,5] Hydrolysis regenerates NO_2^- or HNO_2, except for a small fraction of NO_2 reacting with itself to form some NO_3^-. The determination of quantum yields for the above processes therefore requires the use of OH scavengers. Zafiriou and Bonneau[10] and Zellner *et al.*[11] applied laser flash photolysis with SCN^- as OH scavenger. Optical absorption of the product $(SCN)_2^-$ was used as an indicator for the extent of OH formation in the photodecomposition of NO_2^-. Alif and Boule,[6] who worked with continuous irradiation, employed ethanol or formate anion as scavenger and followed the decrease of nitrite concentration with time to assess the degree of photodecomposition. The data that have resulted from these studies are moderately consistent. Alif and Boule[5] also employed ethanol as scavenger for the determination of OH quantum yields in the photolysis of HNO_2 at two wavelengths, whereas Rettich[7] used ethylene as a scavenger and product glycolaldehyde without wavelength discrimination.

The aim of the present study was to determine quantum yields for processes 1 and 2 as a function of wavelength. Benzene was chosen as OH scavenger because its reaction with OH is rapid and phenol, which is the major product, can be conveniently determined by liquid chromatography. Under these conditions, the primary processes 1 and 2 are expected to be followed by the reactions

$$OH + \text{benzene}\ (+O_2) \rightarrow \text{phenol} + HO_2 \qquad \text{(R3)}$$

$$OH + NO_2^- \rightarrow NO_2 + OH^- \qquad \text{(R4)}$$

$$OH + HNO_2 \rightarrow NO_2 + H_2O \qquad \text{(R5)}$$

By a suitable choice of the concentration ratio $[Bz]/[NO_2^-]$ or $[Bz]/[HNO_2]$ it was possible to make reaction 3 dominant over the two competing reactions. In addition to phenol, nitrate was observed as a secondary product in all our experiments, and the associated quantum yields were determined.

Experimental Section

Spectra and absorption coefficients of nitrite anion and undissociated nitrous acid in aqueous solution were determined with a double beam spectrophotometer against a blank of pure water. Matched quartz cells with an optical path length of 1 cm were used. The spectral resolution in this case was 2 nm (full width at half-peak). The photolysis apparatus combined a 150 W xenon arc lamp with an *f*/2 grating monochromator, whose slits were adjusted to obtain the desired spectral resolution (see below). The light emerging from the monochromator was

[⊗] Abstract published in *Advance ACS Abstracts,* November 1, 1996.

S0022-3654(96)01692-9 CCC: $12.00 © 1996 American Chemical Society

TABLE 1: Decadic Absorption Coefficients for NO_2^- and HNO_2, 2 nm Spectral Resolution

λ (nm)	ϵ_1 (m^2/mol)	ϵ_2 (m^2/mol)	λ (nm)	ϵ_1 (m^2/mol)	ϵ_2 (m^2/mol)
280	0.797	0.092	340	1.90	2.04
282	0.809	0.090	342	1.97	2.33
284	0.820	0.091	344	2.05	2.64
286	0.837	0.091	346	2.13	2.88
288	0.839	0.090	348	2.19	2.79
290	0.850	0.103	350	2.24	2.64
292	0.859	0.120	352	2.27	2.75
294	0.859	0.124	354	2.27	3.25
296	0.862	0.144	356	2.27	3.91
298	0.868	0.174	358	2.24	4.03
300	0.880	0.207	360	2.18	3.79
302	0.884	0.221	362	2.12	3.25
304	0.897	0.252	364	2.02	3.05
306	0.906	0.288	366	1.92	3.26
308	0.926	0.333	368	1.79	3.74
310	0.943	0.376	370	1.66	4.19
312	0.967	0.431	372	1.50	4.15
314	0.996	0.499	374	1.34	3.41
316	1.03	0.574	376	1.18	2.57
318	1.06	0.644	378	1.03	2.11
320	1.11	0.718	380	0.890	2.05
322	1.16	0.836	382	0.751	2.20
324	1.23	0.976	384	0.624	2.41
326	1.29	1.12	386	0.504	2.46
328	1.36	1.18	388	0.402	2.17
330	1.45	1.29	390	0.306	1.57
332	1.53	1.51	392	0.227	0.936
334	1.62	1.76	394	0.173	0.509
336	1.71	1.89	396	0.112	0.262
338	1.81	1.92	398	0.066	0.134
340	1.90	2.04	400	0.045	0.070

refocused to pass first through a thermostated quartz cuvette and then further onto a calibrated thermopile. Ferrioxalate actinometry[12] was additionally used to confirm the calibration of the thermopile. Solutions of nitrite were photolyzed at room temperature at 295 K in a cylindric cuvette 10 cm long, 1.8 cm i.d. (filling capacity 27.3 cm^3); solutions of nitrous acid were photolyzed at 274 K in a cuvette 8 cm long, 1 cm i.d. (filling capacity 7.0 cm^3). The spectral resolution was set to 8 nm (full peak half-width) for the photodecomposition of nitrite anion and 4 nm for that of undissociated nitrous acid. Photon fluxes in the wavelength region 280−390 nm, calculated from the thermopile output, were in the range $(1-7) \times 10^{15}$ photon s^{-1} and $(0.25-1.2) \times 10^{15}$ photon s^{-1}, respectively.

$NaNO_2$ and other chemicals were used as received from commercial suppliers. Deionized (Milli-Q, "organic-free") water was used to prepare solutions. Most solutions were aerated, the concentration of NO_2^- was 5×10^{-4} mol dm^{-3}, and that of benzene was 8×10^{-3} mol dm^{-3}. No particular measures were taken to control pH, but it was observed to adjust to an initial value pH = 6.1 in all runs. A number of experiments were performed with solutions saturated with a mixture of oxygen and nitrous oxide such that their concentrations were 9×10^{-5} and 4.3×10^{-3} mol dm^{-3}, respectively. Aqueous solutions of nitrous acid were prepared from those of $NaNO_2$ by the addition, under vigorous shaking, of 300 mm^3 of 2.5 M sulfuric acid. Thereby the pH was adjusted to about pH = 2. Sulfuric acid was used rather than perchloric acid because the latter gave rise to interference in ion chromatography. All solutions were prepared in Erlenmeyer flasks and pipetted into the photolysis cells. Thereafter the filling ports were capped to prevent evaporative losses.

A Hypersyl ODS 5 column was used to separate by means of high-precision liquid chromatography HNO_2, nitrosophenol, phenol, nitrosobenzene, and benzene. The eluent was a mixture of water and methanol (volume ratio 4:1), and the optical absorption detector was set to 270 nm wavelength. Nitrate was determined by anion chromatography with an aqueous mixture of $NaHCO_3$ and Na_2CO_3 as eluent and two AS4A columns in series in order to achieve a good separation from nitrite or nitrous acid, which elutes ahead of nitrate. The optical absorption detector was set to 215 nm wavelength.

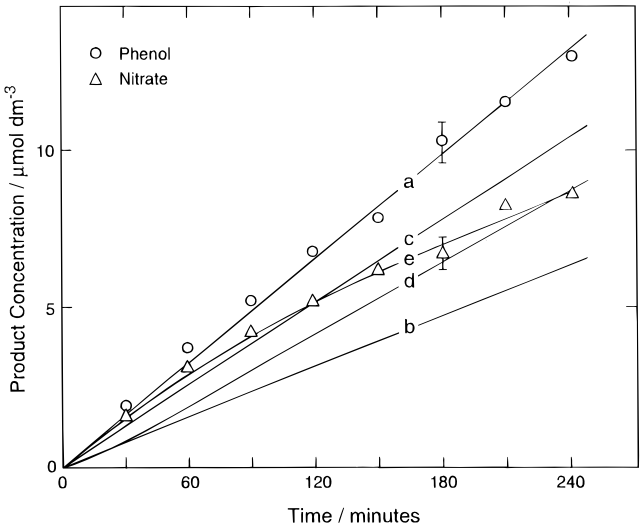

Figure 1. Rise with time of phenol and nitrate in the 355 nm photodecomposition of 5×10^{-4} mol dm^{-3} NO_2^- in the presence of 8×10^{-3} mol dm^{-3} benzene. Vertical bars indicate analytical error ranges. Solid curves show concentrations of nitrate derived by computer simulations based on reactions in Table 4: (a) $k_{11b} = k_{13} = k_{17} = 0$; (b) $k_{13} = k_{17} = 0$, $k_{11b}/k_{11} = 0.4$; (c) $k_{11b}/k_{11} = 0.15$; (d) $k_{11b} = k_{17} = 0$, $k_{13} = 5 \times 10^6$ dm^3 mol^{-1} s^{-1}; (e) $k_{11b} = k_{13} = 0$, $k_{17} = 4 \times 10^4$ dm^3 mol^{-1} s^{-1}.

Results

Absorption Coefficients. Although absorption spectra of nitrite and nitrous acid have been published earlier,[4,6,7,10,11] tabulated data for absorption coefficients appear to be unavailable in the literature. We have therefore redetermined these quantities and present them in Table 1 in 2 nm intervals. The precision of the absorption measurements was 0.2−0.4%, that of wavelength setting 0.5 nm. The total concentration was 1 mmol dm^{-3} in both cases. Decadic absorption coefficients for NO_2^- and HNO_2 were taken at pH 6 and at pH 2, respectively, at 295 K temperature. The values obtained for HNO_2 required a small correction for the presence of about 7% nitrite calculated from the known acid dissociation constant[13,14] $K_1 = [NO_2^-][H^+]/[HNO_2] = 7.6 \times 10^{-4}$ M. Table 1 contains the corrected values. The absorption maxima were found to occur at wavelengths intermediate to those in Table 1: (for NO_2^-) at 355 nm, $\epsilon_1 = 2.28$ m^2 mol^{-1}; (for HNO_2) at 346.5, 357, 371, 385.5 nm, $\epsilon_2 = 2.88$, 4.07, 4.26, 2.50 m^2 mol^{-1}, respectively.

Nitrite Photolysis. Irradiation experiments were carried out at 7 wavelengths in the range 280−390 nm. The total irradiation period was 4 h in each case. The amounts of products observed at the end of this period indicated that less than 3% of nitrite had undergone decomposition. Figure 1 shows the concentration of phenol and nitrate as a function of time during one run at 355 nm. Whereas the rate of phenol formation is essentially constant over the whole irradiation period, that of nitrate formation decreases with time. This behavior was observed also at other wavelengths. Samples of irradiated solutions were analyzed in 30 min intervals. Quantum yields were calculated from the measured product concentrations and the rate of photon absorption according to the equations

TABLE 2: Photolysis of Nitrite: Experimental Conditions, Rates of Formation of Phenol and Nitrate, and Quantum Yields

λ (nm)	ϵ[a] (m^2/mol)	I_o (10^{15} photon/s)	I_{abs} (10^{14} photon/s)	R(Ph)[b] (10^{-10} mol/(L s))	$R(NO_3^-)$[c] (10^{-10} mol/(L s))	$10^2\,\Phi$(Ph)	$10^2\,\Phi(NO_3^-)$	$10^2\,\Phi$(OH)
280	0.793	1.12	0.98	3.54 ± 0.25[d]	3.15 ± 0.24[d]	5.9 ± 0.5[e]	5.3 ± 0.5[e]	$6.8 +0.9/-0.7$[e]
300	0.88	1.42	1.47	5.05 ± 0.25	4.48 ± 0.49	5.9 ± 0.5	5.2 ± 0.5	$6.7 +0.9/-0.7$
320	1.13	1.61	1.93	5.55 ± 0.31	5.31 ± 0.34	4.7 ± 0.4	4.5 ± 0.4	$5.4 +0.7/-0.5$
340	1.89	2.00	3.94	8.09 ± 0.68	6.14 ± 0.49	3.4 ± 0.3	2.6 ± 0.2	$3.8 +0.5/-0.4$
355	2.25	3.12	7.20	9.57 ± 0.73	8.20 ± 0.79	2.2 ± 0.2	1.9 ± 0.2	$2.5 +0.3/-0.3$
370	1.64	4.02	7.00	7.79 ± 0.51	6.38 ± 0.51	1.8 ± 0.2	1.4 ± 0.2	$2.1 +0.3/-0.2$
390	0.328	6.75	2.49	3.30 ± 0.27	2.65 ± 0.29	2.2 ± 0.2	1.7 ± 0.2	$2.5 +0.4/-0.3$

[a] Effective absorption coefficients calculated for 8 nm spectral resolution assuming a triangular monochromator slit function. [b] $n = 8$. [c] $n = 4$. [d] Standard deviation. [e] Includes average measurement errors.

$$\Phi_{Ph} = \alpha f_1 \Phi_{OH} = (VN_L/I_{abs})[\Delta[Ph]/\Delta t] \quad \text{(E1)}$$

$$\Phi_{NO_3} = (VN_L/I_{abs})[\Delta[NO_3^-]/\Delta t] \quad \text{(E1a)}$$

$$I_{abs} = I_o\{1 - 10^{-\epsilon c L}\} \quad \text{(E1b)}$$

where V is the volume of the photolysis cell, $N_L = 6.02 \times 10^{23}$ is the Avogadro constant, $\Delta[Ph]/\Delta t$ and $\Delta[NO_3^-]/\Delta t$, respectively, are the rates of phenol and nitrate formation, and I_{abs} is the rate of photon absorption. I_{abs} was calculated from the measured photon flux I_o, the known absorption coefficient ϵ, the concentration of nitrite c, and the length of the photolysis cell L. Averages for phenol quantum yields were calculated with data from the full 240 min irradiation period (eight data points): nitrate quantum yields were averaged using only data from the first 90 min of irradiation. This gave initial quantum yields and eliminated the influence of reduced rates of nitrate formation at later times. Table 2 provides a summary of the experimental data, average rates of phenol and nitrate formation, and quantum yields obtained at the different wavelengths employed. The phenol quantum yields were used to derive OH quantum yields. As shown in eq 1, both quantities are related by $\Phi_{Ph} = \alpha f_1 \Phi_{OH}$. It is necessary to take into account two factors. One arises from losses of OH by competition between reactions 3 and 4:

$$f_1 = k_3[Bz]/(k_3[Bz] + k_4[NO_2^-]) \quad \text{(E2)}$$

The rate coefficients for the reactions of OH with benzene and nitrite ion are well-known:[15] $k_3 = 7.8 \times 10^9$ and $k_4 = 1 \times 10^{10}$ dm^3 mol^{-1} s^{-1}. With the concentrations applied here, $k_4[NO_2^-]/k_3[Bz] = 8.013 \times 10^{-2}$, and $f_1 = 0.926$. The other correction factor is the yield of phenol from the reaction of OH with benzene, which was previously determined[16] as $\alpha = 0.95 \pm 0.1$. Lower phenol yields have been obtained in γ-radiolysis and pulse radiolysis studies.[17] We prefer the higher value because it was obtained under conditions similar to those used here. The correction factor thus is $(\alpha f_1)^{-1} = 1.137$. The OH quantum yields thus calculated are given in the last column of Table 2.

Additional runs were carried out using solutions saturated with a mixture of nitrous oxide and oxygen. Nitrous oxide as a reagent is commonly used to convert hydrated electrons in aqueous solution to OH radicals by virtue of the fast reaction[15]

$$N_2O + e_{aq}^- (+H^+) \rightarrow N_2 + OH \qquad k_6 = 9.1 \times 10^9\ dm^3\ mol^{-1}\ s^{-1} \quad \text{(R6)}$$

Nitrous oxide thus may serve as a test reagent for the production of hydrated electrons via reaction 1a. Reaction 6 is in competition with reactions of the hydrated electron with NO_2^- and with O_2. Rate coefficients for these reactions are 4.1×10^9 and 1.9×10^{10} dm^3 mol^{-1} s^{-1}, respectively.[15] The concentrations of nitrous oxide and oxygen were adjusted so that the rate of reaction 6 was at least 10 times greater than that of the competing reactions. Irradiations were carried out for 3 h, and OH quantum yields were calculated as before from the observed rates of phenol production, with samples taken every 60 min. Table 3 shows for four wavelengths the averaged OH quantum yields obtained in the presence of N_2O and in N_2O-free solutions. The ratio of both values, 1.076 ± 0.16 on average, is slightly greater than unity, but the error ranges of the OH quantum yields for N_2O-saturated solutions overlap those for N_2O-free solutions. Accordingly, there is no clear-cut evidence for or against the generation of hydrated electrons. The upper limit quantum yield for their formation is 7.6% of the OH quantum yield at each of the four wavelengths.

TABLE 3: Comparison of OH Quantum Yields in Aqueous Solution Saturated with a Mixture of N_2O/O_2 and in Aerated Solution

λ (nm)	N_2O/O_2	aerated	ratio
280	0.073 ± 0.004[a]	0.068 ± 0.008[a]	1.07 ± 0.14[b]
320	0.058 ± 0.003	0.054 ± 0.006	1.07 ± 0.13
355	0.028 ± 0.002	0.025 ± 0.004	1.12 ± 0.19
390	0.026 ± 0.002	0.025 ± 0.004	1.04 ± 0.17
			av 1.076 ± 0.157

[a] Standard deviation. [b] Includes measurement errors.

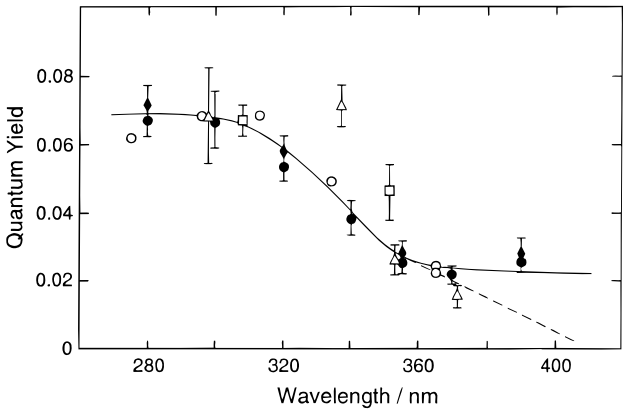

Figure 2. Photodecomposition of nitrite: OH quantum yield versus wavelength. Triangles, ref 10; squares, ref 11; open circles. ref 6; filled circles, present data; diamonds, in the presence of N_2O as scavenger for hydrated electrons. Vertical bars indicate error ranges as far as available. The solid line is a best fit to the data. The dashed line is an empirical extrapolation toward longer wavelengths based on the assumption that quantum yield approaches zero at the onset of the absorption.

Figure 2 summarizes OH quantum yields for the photolysis of nitrite. The present data generally agree well with results from previous studies, especially those of Alif and Boule.[6] Two points (at 337.1 and 351 nm) appear to fall outside the range of the other data. There is no obvious reason for the difference. Interference of scavenger with geminate recombination inside

TABLE 4: Reactions Involved in the Photodecomposition of Nitrite in Aqueous Solution[a]

R1	$NO_2^- + h\nu\ (+H^+) \rightarrow NO + OH$	Φ_1 see text	
R1a	$NO_2^- + h\nu \rightarrow NO_2 + e_{aq}^-$	$\leq 0.076\Phi_1$ see text	
R3	$OH + Bz\ (+O_2) \rightarrow Ph + HO_2$	$k_3 = 7.8 \times 10^9$	ref 15
R4	$OH + NO_2^- \rightarrow OH^- + NO_2$	$k_4 = 1.0 \times 10^{10}$	ref 15
R7	$e_{aq}^- + O_2 \rightarrow O_2^-$	$k_7 = 1.9 \times 10^{10}$	ref 15
R8	$HO_2 = O_2^- + H^+$	$pK_8 = 4.8$	ref 18
R9	$O_2^- + NO \rightarrow ONOO^-$	$k_9 = 6.7 \times 10^9$	ref 19
R10	$ONOO^- + H^+ = ONOOH$	$pK_{10} = 6.6$	refs 20, 21
R11a	$ONOOH \rightarrow NO_3^- + H^+$	$k_{11} = 0.7$	refs 19, 22
R11b	$ONOOH \rightarrow OH + NO_2$	$k_{11b}/k_{11} \leq 0.4$	ref 23
R12	$O_2^- + NO_2 \rightarrow NO_2^- + O_2$	$k_{12} \approx 4.5 \times 10^9$	ref 24
R13	$HO_2/O_2^- + NO_2^- \rightarrow$ products	$k_{13} = 5 \times 10^6$	ref 25
R14	$NO + NO_2 \rightarrow 2NO_2^- + 2H^+$	$k_{14} \approx 1.6 \times 10^8$	ref 26
R15	$NO_2 + NO_2 \rightarrow NO_3^- + NO_2^- + 2H^+$	$k_{15} \approx 8.0 \times 10^7$	refs 26, 27
R16	$2NO + O_2 \rightarrow 2NO_2$	$2k_{16} = 4.2 \times 10^6$	refs 28, 29
R17	$NO_3^- + NO \rightarrow NO_2 + NO_2^-$	$k_{17} \leq 4 \times 10^4$	see text

[a] Rate coefficients are in units of $dm^3\ mol^{-1}\ s^{-1}$ except for reaction 16 ($dm^6\ mol^{-2}\ s^{-1}$) and reaction 11 (s^{-1}).

the solvent cage cannot be held responsible because in all studies the scavenger concentrations were of the same magnitude (~0.1 M, except here, ~0.01 M). However, given the experimental difficulties and error sources in determining absolute OH quantum yields, there is remarkably good agreement between all four data sets. The S-shaped appearance of the wavelength dependence suggests that the data may empirically be represented by a function of the type

$$\Phi_1(\lambda) = a\{1 + \exp(\lambda - \lambda_o)/b\}^{-1} + c \qquad \text{(E3)}$$

A least squares fit program was used to determine the parameters. The solid curve in Figure 2 was obtained with $a = (4.5 \pm 0.3) \times 10^{-2}$, $b = 9.58 \pm 1.65$, $c = (2.3 \pm 0.1) \times 10^{-2}$, and $\lambda_o = 334 \pm 2$.

Table 4 summarizes known reactions that must be considered in the formation of nitrate. At pH ≈ 6, applied in the experiments, HO_2 radicals are almost completely dissociated. Reaction 9 is rapid, so that most of the NO produced is converted to the peroxynitrous anion and thereafter to peroxynitrous acid. A small fraction of NO reacts with NO_2 to yield NO_2^- (reaction 14). At pH 6, peroxynitrous acid is unstable; it mainly isomerizes to form nitrate. This reaction is fast enough to account for the rate of nitrate formation observed initially (compare Figure 1). Computer simulations based on the mechanism shown in Table 4 were performed to determine whether these processes can explain the observed temporal decrease of the rate of nitrate formation apparent in Figure 1. The results did not depend much on whether reactions 1a and 7 were included or not, so that these processes can be ignored. Figure 1 includes some results of the calculations. If reactions 11b and 13 were negligible, nitrate would be formed at a constant rate similar to that of phenol (curve a). The addition of reaction 11b causes the formation rate of nitrate to be lower than that of phenol. The assumption of $k_{11b}/k_{11} = 0.4$ as reported by Yang *et al.*[23] leads to NO_3^- formation at a rate much less than observed (curve b). Our data therefore do not support a high yield of radicals in the decomposition of peroxynitrite. Curve c, which was calculated with $k_{11b}/k_{11} = 0.15$, corresponds to an average $[NO_3^-]/[Ph] \approx 0.77$, similar to that observed. This suggests $k_{11b}/k_{11} \leq 0.15$. Curve d resulted after replacing reaction 11b by reaction 13. Here it was assumed that the product of reaction 13 is NO_2. If O_2^- were the main reactant, a rate coefficient $k_{13} = 5 \times 10^6\ dm^3\ mol^{-1}\ s^{-1}$, as reported by Julien,[25] would cause the rate of nitrate formation to be very low. Accordingly we have assumed nitrite to react with HO_2 using the rate coefficient given. The reaction is initially

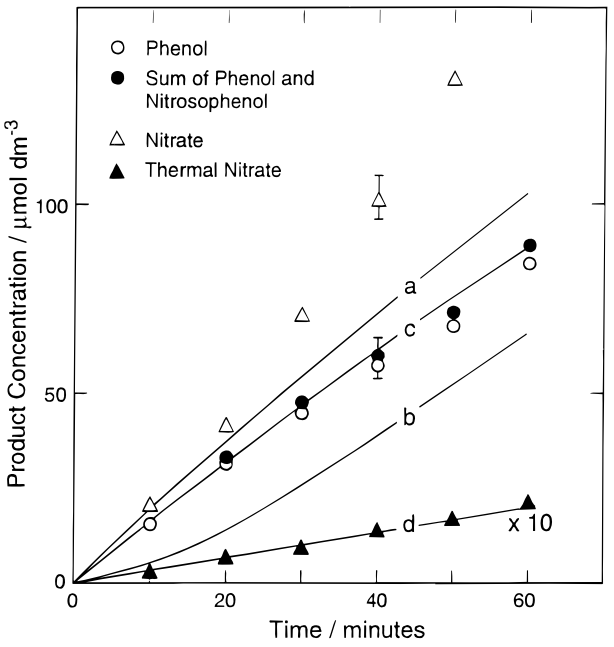

Figure 3. Rise with time of phenol, the sum of phenol and *p*-nitrosophenol, nitrate, and thermal nitrate in the 371 nm photodecomposition of about 5×10^{-4} mol dm^{-3} nitrous acid (pH 2, 274 K) in the presence of 8×10^{-3} mol dm^{-3} benzene. Solid lines show concentrations of nitrate derived by computer simulations based on reactions in Tables 4 and 6: (a) standard run ($k_{13} = k_{17} = k_{20} = k_{20a} = 0$); (b) $k_{13} = 5 \times 10^5$; (c) $k_{20} = 5 \times 10^9$; (d) only thermal reactions (−14, 14, 15, 16).

dominant until sufficient NO builds up to make reaction 9 competitive. This is the cause of the slow initial rate of nitrate formation evident in curve d. None of the processes considered so far can explain the high initial rate of nitrate formation and the decrease in the rate at later times. It appears that a reaction of nitrate with one of the other reactants present in the solution would be required. As an example, we have considered the reaction

$$NO + NO_3^- \rightarrow NO_2 + NO_2^- \qquad \text{(R17)}$$

which we estimate to be endothermic by about 40 kJ mol^{-1} and hence not very convincing. However, curve e in Figure 1, which was obtained by setting $k_{17} = 4 \times 10^4\ dm^3\ mol^{-1}\ s^{-1}$ and neglecting reactions 11b and 13, achieves a better agreement with the experimental data than any of the other assumptions.

Nitrous Acid Photolysis. Experiments were carried out with aerated solutions containing 8×10^{-3} M benzene and 5×10^{-4} M nitrite acidified to pH = 2. The temperature was reduced to 274 ± 0.5 K in order to minimize the thermal decomposition of nitrous acid, which was made evident by the formation of nitrate in the dark. The thermal rise rate of nitrate in such solutions was measured concurrently with irradiation experiments, at the same temperature and in identical cuvettes. The average rate of NO_3^- formation in the dark was found to be $(4.45 \pm 0.50) \times 10^{-10}$ mol $dm^{-3}\ s^{-1}$ as determined from 47 data points in seven runs. This corresponds to an increase in NO_3^- concentration from zero to about 2 μM within 1 h. Except at the shortest wavelengths used, the thermal production of nitrate represented a small fraction of that arising from photodecomposition.

Phenol, *p*-nitrosophenol, and nitrate were observed as HNO_2 photolysis products in the presence of benzene. The fractional concentration of nitrosophenol relative to that of phenol rose linearly with time to 5.5% after 1 h, indicating that nitrosophenol

TABLE 5: Photolysis of Nitrous Acid: Experimental Conditions, Rates of Formation of Phenol and Nitrate, and Quantum Yields

λ (nm)	ϵ[a] (m^2/mol)	I_o (10^{14} photon/s)	I_{abs} (10^{13} photon/s)	R(Ph)[b] (10^{-9} mol/(L s))	R(NO_3^-)[c] (10^{-9} mol/(L s))	10^2 Φ(Ph)	10^2 Φ(NO_3^-)	10^2 Φ(OH)
280	0.148	2.51	0.34	0.22 ± 0.01[d]	0.29 ± 0.03[d]	27.3 ± 2.4[e]	36.0 ± 3.3[e]	34.7 +4.9/−3.7[e]
300	0.249	2.98	0.68	0.48 ± 0.02	0.59 ± 0.07	29.9 ± 2.6	36.8 ± 3.1	36.2 +4.7/−3.5
320	0.762	4.68	3.17	0.29 ± 0.08	2.91 ± 0.16	30.4 ± 2.7	38.6 ± 3.4	34.6 +4.7/−3.5
337.5	1.91	4.96	8.02	6.29 ± 0.17	8.33 ± 0.73	33.1 ± 2.9	43.8 ± 3.6	37.1 +5.0/−3.7
346.5	2.74	6.12	13.6	10.30 ± 0.26	14.60 ± 0.90	31.8 ± 2.7	45.1 ± 3.9	35.5 +4.5/−3.4
357.5	3.74	8.63	25.1	17.10 ± 1.30	28.35 ± 2.00	28.6 ± 2.4	46.3 ± 3.9	31.7 +4.1/−3.1
371	3.85	11.90	35.5	25.18 ± 1.06	37.10 ± 4.70	29.9 ± 2.5	44.0 ± 3.8	32.7 +4.1/−3.1
385.5	2.23	14.40	26.8	21.30 ± 0.82	28.50 ± 2.40	33.5 ± 2.9	44.8 ± 3.9	36.6 +4.6/−3.5

[a] Effective absorption coefficients calculated for 4 nm spectral resolution assuming a triangular monochromator slit function. [b] $4 \le n \le 6$. [c] $n = 4$. [d] Standard deviation. [e] Includes measurement errors.

is a secondary product. Phenol is well-known to react with nitrous acid to give a 95% yield of *p*-nitrosophenol.[30,31] The nitrosating agent is the N_2O_3 intermediate.[29] The concentrations of phenol and *p*-nitrosophenol were added in calculating total phenol quantum yields. Figure 3 shows product concentrations as a function of time during irradiation with light of 357.5 nm wavelength. After 1 h, the concentration of nitrate reaches about 125 μmol dm^{-3}, that is 25% of the initial HNO_2 concentration. Whereas the rate of phenol formation is essentially constant with time, the rate of nitrate formation shows a slight increase.

Although at pH 2 nitrous acid was the major absorbing species, absorption by NO_2^- is not entirely negligible, especially at the shortest wavelengths where the absorption coefficient of nitrous acid is smaller than that of nitrite. The actual concentrations of both species were calculated from the data of Lumme *et al.*[13,14] for the acid dissociation constant K_1 at the prevailing hydrogen ion concentration, ionic strength, and temperature. This gave $[NO_2^-] = 2 \times 10^{-5}$ M and $[HNO_2] = 4.8 \times 10^{-4}$ M.

Five wavelengths used in the irradiation experiments were selected to coincide with the maxima appearing in the HNO_2 absorption spectrum between 330 and 390 nm; the other experiments were conducted with the monochromator set to 280, 300, and 320 nm. Measurements of phenol and nitrate concentrations were made in intervals of 10 min for a total period of 1 h, and individual quantum yields were calculated from eq 1. In calculating average quantum yields a limited data base was used, for which it was assured that the loss of nitrous acid was less than 15% of the initial concentration. Table 5 gives a summary of wavelengths used, absorption coefficients, light fluxes, averaged rates of product formation, and the phenol and nitrate quantum yields obtained. As before, the calculation of OH quantum yields requires application of a factor

$$f_2 = k_3[\mathrm{Bz}]/(k_3[\mathrm{Bz}] + k_4[\mathrm{NO_2}^-] + k_5[\mathrm{HNO_2}])$$

$$= k_3[\mathrm{Bz}]/\{k_3[\mathrm{Bz}] + k_5[\mathrm{HNO_2}](1 + (k_4/k_5)K_1/[\mathrm{H}^+])\} \quad \text{(E4)}$$

to take into account the competition between reactions of OH with benzene, nitrite, and nitrous acid. The rate coefficient for the reaction of OH with HNO_2, which is a hydrogen abstraction reaction, is known only for the gas phase.[32] However, for a number of hydrogen abstraction reactions it has been shown[33,34] that gas phase and aqueous phase rate coefficients are essentially equal. Accordingly, we have used the gas phase rate coefficient at 274 K, $k_5 = 2.6 \times 10^9$ dm^3 mol^{-1} s^{-1}, calculated from the known temperature dependence.[32] The rate coefficient for the reaction between OH and benzene is close to the upper limit imposed by the rate of diffusive transport. The temperature dependence of transport of OH to the reaction site can be assessed from the temperature dependence of the OH quantum yield associated with photodissociation of H_2O_2 in aqueous solution. In this case, diffusion of OH from the photolysis site into the bulk of the solution is in competition with geminate recombination. We have combined data of Hunt and Taube[35] and Baxendale and Wilson,[36] obtained with 254 nm radiation, with the data of Zellner *et al.*,[11] obtained at the wavelengths 308 and 351 nm, to derive an activation energy of 6.29 ± 0.33 kJ mol^{-1}, which reduces the rate coefficient for the reaction of OH with benzene to $k_3 \approx 6 \times 10^9$ dm^3 mol^{-1} s^{-1}. The same procedure gave $k_4 \approx 8 \times 10^9$ dm^3 mol^{-1} s^{-1} at 274 K. With these data, $f_2 = 0.971$, and $(\alpha f_2)^{-1} = 1.084$.

TABLE 6: Supplemental Reactions Involved in the Photodecomposition of Nitrous Acid[a]

R2	$HNO_2 + h\nu \rightarrow NO + OH$	Φ_2 see text	
R5	$OH + HNO_2 \rightarrow H_2O + NO_2$	$k_5 \approx 2.6 \times 10^9$	see text
R-14	$2HNO_2 \rightarrow NO + NO_2$	$k_{-14} = 1.3$ (at 274 K)	ref 26
R18	$HO_2 + NO_2 \rightarrow HOONO_2$	$k_{18} = 1.8 \times 10^9$	ref 24
R19	$HOONO_2 + HNO_2 \rightarrow 2NO_3^- + 2H^+$	$k_{19} \approx 50$	refs 24, 38
R20	$HO_2 + NO \rightarrow ONOOH$	see text	
R20a	$HO_2 + NO \rightarrow OH + NO_2$	see text	

[a] Rate coefficients are in units of dm^3 mol^{-1} s^{-1}.

The OH quantum yields thus calculated still required a correction for OH radicals generated from the photodissociation of nitrite anion. The observed quantum yield is

$$\Phi_{OH} = (\epsilon_1[\mathrm{NO_2}^-]\Phi_1 + \epsilon_2[\mathrm{HNO_2}]\Phi_2)/(\epsilon_1[\mathrm{NO_2}^-] + \epsilon_2[\mathrm{HNO_2}]) \quad \text{(E5)}$$

where the subscripts 1 and 2 refer to nitrite anion and undissociated nitrous acid, respectively. The contribution of OH from the photolysis of nitrite was calculated from the known concentration of $[NO_2^-]$, the absorption coefficients listed in Table 1 corrected for the coarser spectral resolution, and quantum yields taken from Figure 2 (solid line). At the shortest wavelength used, 280 nm, the correction term contributed about 5% to the total OH quantum yield, and at 320 nm it was smaller than 1%. The corrected OH quantum yields are shown in the last column of Table 5. The data show remarkably little dependence on wavelength. The average value for the wavelength range 280−385 nm is $\Phi_2 = 0.35$ with a standard deviation of ± 0.02, which is less than the range of measurement errors indicated in Table 5.

An explanation of nitrate formation at pH 2 requires reactions supplementing those in Table 4.

The additional reactions are listed in Table 6. At pH 2 the concentration ratio $[O_2^-]/[HO_2] \approx 1.3 \times 10^{-3}$ so that reaction 9 is still competitive, whereas reaction 12 can be ignored in comparison to 18. Reaction 20 is the equivalent of reaction 9, but there exists no information on its rate coefficient or product distribution. Computer calculations were carried out to explore the behavior of the system. The data of Park and Lee[26] were extrapolated to estimate rate coefficients $k_{-14} = 1.3$ s^{-1}, $k_{14} =$

2×10^8, and $k_{15} = 1 \times 10^8$ dm^3 mol^{-1} s^{-1} at $T = 274$ K. The rate coefficient for reaction 11 at 274 K was taken from Benton and Moore,[37] $k_{11} = 5 \times 10^{-2}$ s^{-1}.

The dark formation of nitrate, which involves the thermal decomposition of nitrous acid (reaction −14) followed by reactions 14, 15, and 16, was found to give a constant rate of nitrate production. The observed rate of nitrate formation was reproduced when an equilibrium constant $K_{14} = k_{14}/k_{-14} = 1.6 \times 10^8$ dm^3 mol^{-1} s^{-1} was adopted, which agrees well with the data of Park and Lee[26] extrapolated to 274 K, but not with the lower value for the rate coefficient $k_{14} = 7.4 \times 10^6$ dm^3 mol^{-1} s^{-1} reported by Grätzel *et al.*[39] Concentrations of NO and NO_2 were stationary under these conditions: [NO] $\approx 6.8 \times 10^{-7}$ mol dm^{-3} and [NO_2] $\approx 2.2 \times 10^{-9}$ mol dm^{-3}. Figure 3 includes results for the dark formation of nitrate, observed and calculated.

A standard run of computer simulations included reactions 2, 3, 5, 9, 11, 18, and 19 plus those active in the thermal decomposition of HNO_2, −14, 14, 15, and 16. The results are included in Figure 3 (curve a). Under these conditions the formation rate of nitrate is about 15% higher than that of phenol and approximates the observed initial rise rate (but not the increase at later times). Two-thirds of nitrate derive from reaction 19, that is via the formation of peroxynitric acid in reaction 18; the remainder is mainly due to the decomposition of peroxynitrous acid formed in reaction 9. The addition of reaction 13 with an assumed $k_{13} = 5 \times 10^5$ dm^3 mol^{-1} s^{-1} reduced the rate of nitrate formation substantially (curve b), primarily by lowering the yield of peroxynitric acid. In all these cases, the addition of reaction 17 did not result in significant changes; the time period of 1 h is too short. This contrasts with the photolysis of nitrite, where longer irradiation times were applied.

In the gas phase, the reaction of HO_2 with NO is well-known to produce NO_2 and OH radicals;[40] in the aqueous phase it is expected to form mainly peroxynitrous acid. If the rate coefficient of reaction 20 in the aqueous phase were the same as in the gas phase, its value would be $k_{20} + k_{20a} \approx 5 \times 10^9$ dm^3 mol^{-1} s^{-1}. We consider this an upper limit, because many reactions of HO_2 are slower than the corresponding reactions of O_2^- radicals.[18] Although Table 6 includes both channels of reaction 20, one would expect little difference whether OH radicals were produced from reaction 20a or 11b. Computer simulations confirmed this expectation. However, reaction 11b was not found to be very prominent in the photolysis of nitrite. The effect of adding reaction 20 was explored, first with $k_{20} = 5 \times 10^9$ dm^3 mol^{-1} s^{-1} and $k_{20a} = 0$, then with $k_{20} = 0$ and $k_{20a} = 5 \times 10^9$ dm^3 mol^{-1} s^{-1}. In both cases the formation rate of nitrate was similar to that of phenol. The second case resulted in a chain reaction where the chain length is determined by the partitioning of HO_2 between reaction 18 (chain terminating) and reaction 20a (chain propagating), the partitioning depending on the steady state concentrations of NO and NO_2. Under conditions of low rates of light absorption (at short wavelengths) the thermal decomposition of HNO_2 was a significant source of NO and NO_2 and chain lengths of about 600 were calculated, whereas high rates of light absorption, such as at 371 nm, reduced the chain length to less than 10. If reaction 20a were important, the primary OH quantum yields derived from the measurements would have to be appropriately reduced, by a factor of about 600 at short wavelengths compared to a factor of about 10 at long wavelengths. A decrease of the primary quantum yield by a factor of 60 when going from longer toward shorter wavelengths is considered extremely unlikely. This result provides a strong argument against a significant occurrence of reaction 20a.

The results of the computer simulations suggest that in order to approximate the observed high yield of nitrate, the formation rate of $HOONO_2$ must be further increased at the expense of the formation of HOONO. This requires that reactions 20 and 20a are essentially negligible. Appropriate experiments would be necessary to substantiate our conclusion. Finally, we have also considered the possibility that the deposition of energy by light absorption may have raised the temperature of the solution and thereby increased the rate of thermal HNO_2 decomposition. However, the calculated temperature rise of 0.01 K is insignificant.

Atmospheric Implications. The measured absorption coefficients and quantum yields were used to calculate photodissociation frequencies for processes 1 and 2 in the troposphere for midday summer clear sky conditions at about 50° northern latitude. The two quantities are given by

$$j_1(\mathrm{OH}) = \int \Phi_1(\lambda)\, \sigma_1(\lambda)\, I(\lambda)\, \mathrm{d}\lambda \qquad \text{(E6a)}$$

$$j_2(\mathrm{OH}) = \int \Phi_2(\lambda)\, \sigma_2(\lambda)\, I(\lambda)\, \mathrm{d}\lambda \qquad \text{(E6b)}$$

where $\sigma_1(\lambda)$ and $\sigma_2(\lambda)$ are the corresponding absorption cross sections, defined by $\sigma_x(\lambda) = (\epsilon_x/N_A)$ ln 10 with $N_A = 6.02 \times 10^{23}$ (Avogadro's number); $I(\lambda)$ is the actinic solar photon flux, and the integration must be performed over the entire photochemically active wavelength region. Inside atmospheric water drops the actinic solar flux may be nearly doubled due to internal reflections.[41,42] This effect is neglected here. The solar flux was calculated in 5 nm intervals by the two-stream method of Brühl and Crutzen,[43] which includes backscattered light and a ground albedo 0.25. A standard ozone profile was adopted in the calculation. The zenith angle was set to 25°, which corresponds to noontime summer conditions at 48° latitude. The absorption coefficients in Table 1 were averaged over 5 nm wavelength intervals to make them compatible with the solar flux data. The photodissociation coefficients derived are $j_1(\mathrm{OH}) = 3.7 \times 10^{-5}$ s^{-1} and $j_2(\mathrm{OH}) = 6.8 \times 10^{-4}$ s^{-1}. In the case of NO_2^- the data in Figure 2 possibly allow a stronger decline of the quantum yield at wavelengths longer than 370 nm than shown by the solid interpolation curve. However, the photodissociation frequency calculated with quantum yields declining in a linear manner from $\Phi_1(\mathrm{OH}) = 0.02$ at 370 nm to $\Phi_1 = 0$ at 420 nm (shown in Figure 2 by the broken line) is essentially the same as that given above.

Discussion

Most absorption spectra published previously are difficult to evaluate for comparison with the present data (Table 1) except those given by Alif and Boule.[6] Their data as read from the graph and our results are in reasonable agreement. Alif and Boule[6] reported the following numerical values for coefficients at the absorption maxima: $\epsilon_1 = 2.2$ m^2 mol^{-1} at 352 nm (for NO_2^-) and $\epsilon_2 = 4.8$ and 5.0 m^2 mol^{-1} at 358 and 371 nm, respectively, for two of the principal absorption maxima of HNO_2. The spectral resolution was not given. The present results for the same absorption maxima are (NO_2^-) $\epsilon_1 = 2.28$ m^2 mol^{-1} at 355 nm and $\epsilon_2 = 4.07$ and 4.26 m^2 mol^{-1} at 357 and 371 nm, respectively. In the latter cases the values of Alif and Boule are 17% higher than ours. The spectrum of HNO_2 in aqueous solution resembles that in the gas phase,[44] but the peaks are broader and the distinction between cis- and trans-rotamers, which in the gas phase give rise to separate progressions, is lost. Compared with absorption cross sections for HNO_2 in the gas phase, reported by Bongartz *et al.*[44] with 0.1

nm spectral resolution, the values for the maxima of HNO_2 in aqueous solution are by a factor of about 3.3 lower, whereas the minima are higher. The difference is mainly due to collisional broadening, not so much to the coarser spectral resolution used here.

Results for OH quantum yields associated with the photodecomposition of NO_2^- largely confirm the data that were reported previously,[6,10,11] but the present results add information in that most wavelengths are different from those used previously. The agreement is good in view of the fact that different scavengers and continuous irradiation as well as laser flash photolysis techniques have been employed. As discussed by Zafiriou and Bonneau,[10] the O^-/OH quantum yield is determined by several competing processes, such as dissociation from the excited state versus internal conversion of energy toward lower lying, nondissociating states and geminate recombination of the dissociation products versus their escape from the solvent cage. Only the latter process is observed. The observation of OH formation at the long wavelength threshold of absorption indicates that sufficient kinetic energy is provided to the dissociation products to allow a fraction of them to leave the solvent cage. The rise of the quantum yield toward lower wavelengths (increasing energy) may be due to two effects: additional kinetic energy being imparted to the dissociation products, so that the probability of escape from the solvent cage is increased, and/or an increase in the rate of dissociation of the excited state occurs compared to that of internal energy conversion. The latter process must be responsible for the limit of the quantum yield approached at short wavelengths. Zellner *et al.*[11] have explored the temperature dependence of OH quantum yields at the wavelengths 308 and 351 nm and reported activation energies of 13 ± 3 and 15 ± 3 kJ mol^{-1}, respectively, indicating that the temperature dependence does not depend on wavelength. The values are similar to that obtained for the OH quantum yield from the photodecomposition of nitrate,[11] but markedly higher than that for the photodissociation of H_2O_2 (6.29 ± 0.33 kJ mol^{-1}; see the Results section). The difference suggests the existence of an additional energy barrier for O^- compared to OH, presumably caused by the charge of O^- and its interaction with the solvent. If O^- were neutralized promptly after formation, it would leave the solvent cage as OH and the temperature dependence should be the same as that for OH. Therefore, the data indicate that protonation of O^- occurs after the radical has left the solvent cage.

The scavengers used in this study and by Alif and Boule[6] lead to the formation of O_2^-. The agreement between the two data sets would be much less satisfactory if the peroxynitrous acid product expected to arise from the reaction of O_2^- with NO generated a significant fraction of OH radicals, because it would require corrections whereby our quantum yields would have to be lowered, whereas those of Alif and Boule would have to be raised. The laser photolysis experiments do not involve O_2^- radicals. Yet the majority of these data agree with those derived from the steady state irradiation experiments. This suggests that the yield of OH radicals in the decomposition of HOONO must be small.

Values for OH quantum yields from the photodecomposition of HNO_2 have not been reported previously, but quantum yields for the rate of HNO_2 disappearance in the presence of a scavenger have been determined. Alif and Boule[6] used solutions of 2×10^{-2} mol dm^{-3} HNO_2 at pH 1.4 with 0.1 mol dm^{-3} formate added as scavenger; quantum yields obtained at two wavelengths, 254 and 365 nm were 0.46 ± 0.1 and 0.45 ± 0.1, respectively. The values are surprisingly similar, although they refer to two different absorption regimes. The disappearance of HNO_2 corresponds to the production of nitrate observed in the present study. Comparison with the data in Table 5 shows that at wavelengths in the vicinity of 365 nm our NO_3^- quantum yields are in good agreement with the quantum yield for HNO_2 reported by Alif and Boule.[6] These authors do not mention any corrections for the thermal decomposition of nitrous acid, which may have been appreciable.

Rettich[7] used UV radiation spanning the wavelength range 300−400 nm, with the light intensity centered at 350 nm. Ethylene was the scavenger; glycolaldehyde and hydroxylamine were produced in approximately equimolar amounts for each mole HNO_2 disappearing. The products were explained to arise from the addition of OH radicals to the double bond of ethylene, followed by a further addition of NO, rearrangement of the intermediate to form an oxime, and its hydrolysis. The reaction of OH with ethylene was in competition with the reaction of OH with HNO_2. Therefore, the ethylene concentration was kept constant at 6 mmol dm^{-3} and the nitrous acid concentration was varied between 3 and 7 mmol dm^{-3}. The quantum yields for HNO_2 disappearance were extrapolated to zero HNO_2 concentration to obtain a limiting quantum yield of 0.095. Assuming the proposed reaction mechanism to be correct, ethylene as scavenger would avoid the formation of HO_2 radicals. Even if in the presence of oxygen β-hydroxyethylperoxy radicals were formed, the yield of HO_2 radicals from subsequent reactions would be smaller than that from formate or benzene. Accordingly, the OH quantum yield inferred by Rettich[7] provides a lower limit to the true value over a fairly broad wavelength range. The value is by a factor of about 3.5 lower than that obtained here with benzene as scavenger, which may indicate the occurrence of a short chain reaction involving OH formed either in a reaction between HO_2 and NO or in the decomposition of HOONO. On the other hand, the quantum yields for photodissociation of HNO_2 and H_2O_2 in aqueous solution are expected to be fairly similar, because both compounds feature gas phase quantum yields close to unity,[9,35] and the yield in solution depends mainly on the rate of diffusion of OH leaving the solvent cage, which is in competition with geminate recombination. The quantum yield for H_2O_2 photodissociation in aqueous solution[11,35,36] is about 0.5. Therefore, a OH quantum yield of 0.35 for HNO_2 photodissociation is reasonable, whereas a quantum yield near 0.1 would require further interpretation.

Difficulties were experienced in the present study to reproduce by computer calculations based on known reactions the rates of nitrate formation in the photolyses of both NO_2^- and HNO_2 for extended irradiation periods. In the first case the calculated rates were somewhat higher than observed; in the second case they were lower. The discrepancies indicate that the reactions involving nitrogen oxides and the corresponding acids in aqueous solution are not well understood and require further study.

In atmospheric water drops, the photodecomposition of NO_2^- is in competition with the oxidation of NO_2^- by reaction with ozone. We assume an ozone mole fraction of 3×10^{-9} in the surrounding air. The known Henry's law coefficient for ozone[45] in water is 1.6×10^{-2} mol dm^3 atm^{-1}, and the rate coefficient for the reaction[46] is 5×10^5 dm^3 mol^{-1} s^{-1}, both at 283 K. The reaction frequency, 7.3×10^{-5} s^{-1}, is by a factor of 2 larger than the calculated photodissociation frequency, 3.7×10^{-5} s^{-1}, which was maximized by assuming midday summer conditions. The sum of both rates suggests an e-fold lifetime of about 3 h for NO_2^- in sunlit atmospheric water drops. Nitrite in the atmosphere has been observed primarily in ground clouds with concentrations in the range[1,2] 0.7−40 μmol dm^{-3}. The higher

concentrations would provide a significant source of OH radicals in the aqueous phase (2.6×10^{-11} to 1.5×10^{-9} s^{-1}) compared to the rate of OH intrusion from the gas phase, estimated[47,48] to be about 1×10^{-9} s^{-1}. The photodissociation frequency for undissociated nitrous acid is by an order of magnitude greater than that for the nitrite anion. However, HNO_2 is quite volatile so that it tends to escape to the gas phase when cloud water is acidified to pH values ≤ 4. The Henry's law coefficient[26] for HNO_2 is about 49 mol dm^{-3} atm^{-1}. For a liquid water volume ratio in air of 10^{-6} and an aqueous solution at pH 2 one estimates that more than 99% of the HNO_2 would reside in the gas phase. Since the photodissociation coefficients in both phases are similar in magnitude, photolysis in the aqueous phase will be negligible compared to that in the gas phase.

Acknowledgment. This study, a contribution to EUROTRAC Subproject HALIPP, has received support from the Deutsche Forschungsgemeinschaft within the program of Sonderforschungsbereich 233 (Dynamics and Chemistry of Hydrometerors).

References and Notes

(1) Cape, J. N.; Hargreaves, K. J; Storeton-West, R.; Fowler, D.; Colville, R. N.; Choularton, T. W.; Gallagher, M. W. *Atmos. Environ.* **1992**, *26A*, 2301−2307.

(2) Lammel, G.; Gieray, R. In *Physico-Chemical Behaviour of Atmospheric Pollutants*, Angeletti, G., Restelli, G., Eds.; Proc. 6th European Symp., Varese, Italy; European Commission: Luxembourg, 1994; pp 975−981.

(3) Sharp, J. H. In *Nitrogen in the Marine Environment*, Carpenter, E. J., Capone, D. G., Eds.; Academic Press: New York, 1983; pp 1−35.

(4) Treinin, A.; Hayon, E. *J. Am. Chem. Soc.* **1970**, *92*, 5821−5828.

(5) Strehlow, H.; Wagner, I. *Z. Phys. Chem. N. F. (Frankfurt)* **1982,** *132*, 151−160.

(6) Alif, A.; Boule, P. J. *Photochem. Photobiol.* **1991,** *A59*, 357−367.

(7) Rettich, T. R. Some Photochemical Reactions of Aqueous Nitrous Acid. Ph.D. Thesis, Dept. of Chemistry, Case Western Reserve University, 1978.

(8) Cox, R. A. *J. Photochem.* **1974**, *3*, 175−188.

(9) Cox, R. A.; Derwent, R. G. *J. Photochem.* **1976**, *6*, 23−34.

(10) Zafariou, O. C.; Bonneau, R. *Photochem. Photobiol.* **1987,** *45*, 723−727.

(11) Zellner, R.; Exner, M.; Herrmann, H. *J. Atmos. Chem.* **1990,** *10*, 411−425.

(12) Hatchard, C. G.; Parker, C. A. *Proc. R. Soc.* **1956** *A235*, 518−536.

(13) Lumme, P.; Tummavuori, J. *Acta Chem. Scand.* **1965,** *19*, 617−621.

(14) Lumme, P.; Lahermo, P.; Tummavuori, J. *Acta Chem. Scand.* **1965,** *19*, 2175−2188.

(15) Buxton, G. V.; Greenstock, V.; Hellman, C. L.; Ross, A. B. *J. Phys. Chem. Ref. Data* **1988,** *17*, 513−886.

(16) Deister, U.; Warneck, P.; Wurzinger, C. *Ber. Bunsen-Ges. Phys. Chem.* **1990**, *94*, 594−599.

(17) Pan, X.-M.; Schuchmann, M. N.; von Sonntag, C. *J. Chem. Soc., Perkin Trans.* **1993**, *2*, 289−297.

(18) Bielski, B. H. J.; Cabelli, D. E.; Arudi, R. L.; Ross, A. B. *J. Phys. Chem. Ref. Data* **1985**, *14*, 1041−1100.

(19) Huie, R. E.; Padmaja, S. *Free Rad. Res. Commun.* **1993**, *18*, 195−199.

(20) Keith, W. G.; Powell, R. E. *J. Chem. Soc.* **1969**, *A1969*, 90.

(21) Drexel, C.; Elias, H.; Fecher, B.; Wannowius, K. J. *Fresenius, J. Anal. Chem.* **1991**, *340*, 605−615.

(22) Hughes, M. N.; Nicklin, H. G. *J. Chem. Soc.* **1968**, *A1968*, 450−452.

(23) Yang, G.; Candy, T. E.; Boaro M.; Wilkin, H. E.; Jones, P.; Nazhat, N. B.; Saadalla-Nazhat, R. A.; Blake, D. R. *Free Radical Biol. Med.* **1992**, *12*, 327−330.

(24) Logager, T.; Sehested, K. *J. Phys. Chem.* **1993**, *97*, 10047−10052.

(25) Julien, R. *Int. J. Radiat. Phys. Chem.* **1975**, *7*, 2142−2147.

(26) Park, J.-Y.; Lee, Y.-N. *J. Phys. Chem.* **1988**, *92*, 6294−6302.

(27) Grätzel, M.; Henglein, A.; Lilie, F.; Beck, G. *Ber. Bunsen-Ges. Phys. Chem.* **1969**, *73*, 646−653.

(28) Awad, H. H.; Stanbury, D. M. *Int. J. Chem. Kinet.* **1993**, *25*, 375−381.

(29) Pires, M.; Rossi, M. J.; Ross, D. S. *Int. J. Chem. Kinet.* **1994**, *26*, 1207−1227.

(30) Veibel, S. *Ber. Dtsch. Chem. Ges.* **1930**, *63*, 1577−1589.

(31) Challis, B. C.; Lawson, A. J. *J. Chem. Soc.* **1971**, *1971B*, 770−775.

(32) Jenkin, M. E.; Cox, R. A. *Chem. Phys. Lett.* **1987**, *137*, 548−552.

(33) Güsten, H.; Filby, L. G.; Schoof, S. *Atmos. Environ.* **1981**, *15*, 1763−1765.

(34) Klöpffer, W.; Kaufmann, G.; Frank, R. *Z. Naturforsch.* **1985**, *40a*, 686−692.

(35) Hunt, J. P.; Taube, H. *J. Am. Chem Soc.* **1952**, *74*, 5999−6002.

(36) Baxendale, J. H.; Wilson, J. A. *Trans. Faraday Soc.* **1956**, *53*, 344−356.

(37) Benton, D. J.; Moore, P. *J. Chem Soc.* **1970**, *A1970*, 3179−3182.

(38) Elias, H.; Wannowius, K. J.; Steingens, U., Private communication, Technische Hochschule Darmstadt, Germany.

(39) Grätzel, M.; Taniguchi, S.; Henglein, A. *Ber. Bunsen-Ges. Phys. Chem.* **1970**, *74*, 488−492.

(40) Atkinson, R.; Baulch, D. L.; Cox, R. A.; Hampson, Jr.; Kerr, J. A.; Troe, J. *J. Phys. Chem. Ref. Data* **1989**, *18*, 881−1097.

(41) Madronich, S. *J. Geophys. Res.* **1987**, *92*, 9740−9752.

(42) Bott, A.; Zdunkowski, W. *J. Opt. Soc. Am.* **1987**, *4A*, 1361−1365.

(43) Brühl, C.; Crutzen, P. C. *Geophys. Res. Lett.* **1989**, *16*, 703−706.

(44) Bongartz, A.; Kames, J.; Welter, F.; Schurath, U. *J. Phys. Chem.* **1991**, *95*, 1076−1082.

(45) Kozak-Channing, L. F.; Heltz, G. R. *Environ. Sci. Technol.* **1983**, *17*, 145−149.

(46) Damschen, D. E.; Martin, D. L. *Atmos. Environ.* **1983**, *17*, 2005−201.

(47) Jacob, D. J.; Gottlieb, E. W.; Prather, M. J. *J. Geophys. Res.* **1989**, *94*, 12975−13002.

(48) Lelieveld, J.; Crutzen, P. J. *Nature* **1990**, *343*, 227−233.

JP961692+